Instrumentation for the upgrade to the JET core charge-exchange spectrometers

Cite as: Rev. Sci. Instrum. 89, 10D113 (2018); https://doi.org/10.1063/1.5037639 Submitted: 26 April 2018 . Accepted: 06 June 2018 . Published Online: 28 August 2018

N. C. Hawkes, E. Delabie , S. Menmuir, C. Giroud, A. G. Meigs, N. J. Conway, T. M. Biewer , D. L. Hillis, and JET Contributors

COLLECTIONS

Paper published as part of the special topic on Proceedings of the 22nd Topical Conference on High-Temperature Plasma Diagnostics

Note: Paper published as part of the Proceedings of the 22nd Topical Conference on High-Temperature Plasma Diagnostics, San Diego, California, April 2018.







ARTICLES YOU MAY BE INTERESTED IN

JET diagnostic enhancements testing and commissioning in preparation for DT scientific campaigns

Review of Scientific Instruments 89, 10K119 (2018); https://doi.org/10.1063/1.5038548

Determination of 2D poloidal maps of the intrinsic W density for transport studies in JET-II W

Review of Scientific Instruments 89, 113501 (2018); https://doi.org/10.1063/1.5046562

Extensions to the charge exchange recombination spectroscopy diagnostic suite at ASDEX Upgrade

Review of Scientific Instruments 88, 073508 (2017); https://doi.org/10.1063/1.4993131







Instrumentation for the upgrade to the JET core charge-exchange spectrometers

N. C. Hawkes, ^{1,a)} E. Delabie, ² S. Menmuir, ¹ C. Giroud, ¹ A. G. Meigs, ¹ N. J. Conway, ¹ T. M. Biewer, ² D. L. Hillis, ² and JET Contributors ^{3,b)}

(Presented 18 April 2018; received 26 April 2018; accepted 6 June 2018; published online 28 August 2018)

Charge-exchange spectroscopy on JET has become particularly challenging with the introduction of the ITER-like wall. The line intensities are weaker and contaminated by many nuisance lines. We have therefore upgraded the instrumentation to improve throughput and allow the simultaneous measurement of impurity and fuel-ion charge exchange by splitting the light between two pairs of imaging spectrometers using dichroic beam splitters. Imaging instruments allow us to stack 11 × 1 mm diameter fibres on the entrance slits without cross talk. CCD cameras were chosen to have 512 × 512 pixels to allow frame transfer times <0.2 ms which with minimum exposure times of 5 ms give tolerable smearing even without a chopper. The image plane is optically demagnified 2:1 to match the sensor size of these cameras. Because the image plane of the spectrometer is tilted, the CCD must also be tilted to maintain focus over the spectrum (Scheimpflug condition). To avoid transverse keystoning (causing the vertical height of the spectra to change across the sensor), the configuration is furthermore designed to be telecentric by a suitable choice of the lens separation. The lens configuration is built almost entirely from commercial off-the-shelf components, which allowed it to be assembled and aligned relatively rapidly to meet the deadline for in-vessel calibration in the JET shutdown. https://doi.org/10.1063/1.5037639

I. INTRODUCTION

In preparation for the construction of ITER, in 2011, the JET experiment installed a fully metallic first wall; prior to this, extensive use was made of refractory carbon fibre composite components (CFCs). With this modification, the majority of the plasma facing components were replaced with either bulk beryllium or beryllium coated CFCs. The divertor tiles were replaced with a mixture of bulk tungsten and tungsten overcoated CFC tiles. These changes have had a detrimental impact on our ability to measure impurity ion parameters: temperature $(T_{\rm I})$, density $(n_{\rm I})$, and velocity (v_{ϕ}) via charge-exchange spectroscopy. Charge-exchange spectroscopy on JET had, up to this point, made routine use of the carbon n = 8-7 transition ¹ as a bright spectral line in a part of the spectrum unaffected by nuisance lines. Reduction in the level of carbon in the plasma, by an order of magnitude, is one reason for the difficulties in analysis. The other problem has been the appearance of very many weak spectral lines (often tungsten) throughout the spectral region used for carbon spectroscopy.² With the introduction of so much beryllium into the machine, the beryllium charge-exchange (Be n = 6-5 etc.) features are somewhat more intense, but the beryllium spectrum is complicated by edge emission lines of Be and C so that beryllium charge-exchange does not provide an adequate substitute for the carbon spectra.

Two strategies have been applied which are successful in improving the measurements: modulation (typically with a 90% "ON" time) of the neutral beams to help discriminate the active charge-exchange signal from the various interfering nuisance lines and adding low levels of neon to the discharge so as to be able to make measurements of the Ne n = 11-10 transition. The neon transition is still affected by nuisance lines, and using these two techniques in tandem offers a further improvement over either technique alone. However, there is a (small) penalty on plasma performance due to the neutral beam power from one or more sources being off for 10% of the time or due to the extra radiated power associated with the introduction of low levels of neon into the plasma.

An alternative to the above techniques is to measure the charge-exchange feature of the fuel ions—the D_{α} spectrum. This line is bright in comparison to impurity charge-exchange emission but overlaps with a strong low temperature feature from the plasma edge and beam emission features from the Stark emission of the moving beam ions. Prompted by promising results achieved in fitting beam emission³ and successes elsewhere⁴ in fitting this complex spectrum, this technique was recently applied to JET spectra with considerable success.⁵ Modulation is helpful in removing passive emission, but a minimum of 11 free parameters is still required to capture all the variables in the active D_{α} spectrum. The neutral

¹UKAEA/CCFE, Culham Science Centre, Abingdon OX14 3DB, United Kingdom

²Oak Ridge National Laboratory, Oak Ridge, Tennessee 37831-6169, USA

³EUROfusion Consortium, JET, Culham Science Centre, Abingdon OX14 3DB, United Kingdom

Note: Paper published as part of the Proceedings of the 22nd Topical Conference on High-Temperature Plasma Diagnostics, San Diego, California, April

a)nick.hawkes@ukaea.uk

b) See the author list of X. Litaudon et al., Nucl. Fusion 57, 102001 (2017).

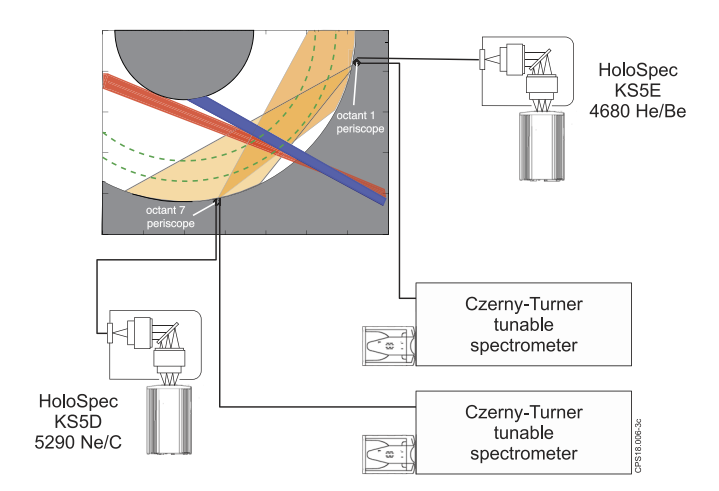


FIG. 1. Layout of core charge-exchange spectrometers the on JET *prior to the upgrade:* the upgrade involves replacing the two Czerny-Turner wavelength-tunable spectrometers with pairs of Isoplane instruments covering the main ion and impurity wavelengths simultaneously. The two HoloSpec instruments are unchanged.

beam and line of sight geometries, Fig. 1, are such that for one set of sightlines the Doppler shift of the beam emission, which overlaps with one of the wings of the charge-exchange line, is increasing with radius while for the other set it is decreasing. As a result, the spectra from one periscope are better for diagnosing the core, whereas the other is better suited for mid-radius to the pedestal top. To exploit the main ion charge-exchange signals, the spectrometers have had to be tuned away from the carbon and beryllium spectra and so choices are made a priori as to the best strategy to adopt for any particular plasma scenario. To avoid this limitation, we have designed an arrangement that uses pairs of spectrometers and dichroic beamsplitters to allow us to measure both the main ion and the impurity charge-exchange spectra simultaneously from both co- and counter-NBI lines of sight. This will have the further benefit that we will be able to constrain the two measurements to fit to a common ion temperature (subject to issues of equipartition, cross section corrections, etc.) which should reduce the errors compared to independent fits.

II. OVERVIEW OF THE UPGRADE

The JET charge-exchange spectrometer suite is furnished with two views of the neutral beam system, Fig. 1, one red and one blue shifted.^{6,7} Each of the views has two arrays of 15 fibres covering from beyond the outboard edge of the plasma to inboard of the magnetic axis. One array from the red-shifted direction is connected to a Kaiser HoloSpec f/1.8 fixed wavelength spectrometer⁸ and a Roper Cascade 512B CCD camera monitoring the spectral region of 468 nm for helium and beryllium emission.⁹ This is complemented by a tunable spectrometer connected to one array from the blue-shifted direction, routinely set to also monitor the He/Be spectrum. Conversely, the other blue-shifted array is connected to a HoloSpec monitoring the carbon and neon spectrum around 529 nm with a tunable spectrometer looking from the opposite direction and routinely tuned to the same spectral region.

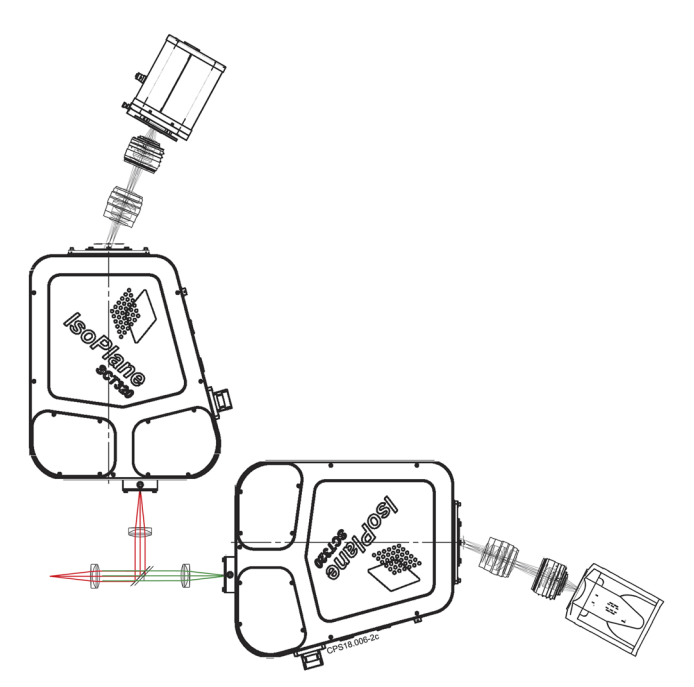


FIG. 2. Layout of one pair of the new spectrometers. Each pair replaces one of the Czerny-Turners in Fig. 1.

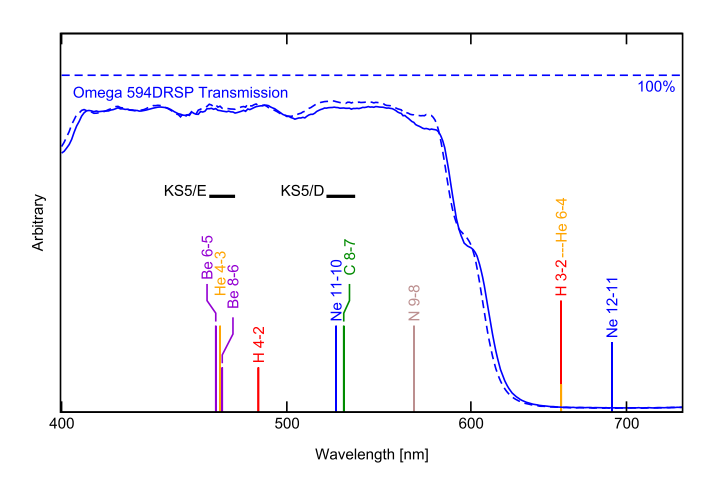


FIG. 3. Measured filter transmittance curves (two samples). The bars marked KS5/D and KS5/E show the wavelength ranges of the two HoloSpec fixed wavelength spectrometers. Some of the important charge-exchange wavelengths are marked with "sticks." Wavelengths above 600 nm are reflected into the long-wavelength spectrometers.

The aim of this upgrade was to replace each of the single tunable spectrometers with a pair of instruments, Fig. 2, able to measure simultaneously the wavelength regions above 600 nm for D_{α} and below for the light impurities (C, Be, He, Ne, N). For each view, a dichroic filter splits the light between the two spectrometers at 600 nm, as shown in Fig. 3 and described in Sec. III.

III. INPUT OPTICS

An off-the-shelf short-pass dichroic filter, Omega part number 594DRSP, was selected and its transmission response was measured with a scanning monochromator (Bentham model IDR300-PSL), Fig. 3.

FIG. 4. Detail of spectrometer sensitivity response with modulation caused by etaloning in the input filter, blue. After adjusting the input lenses (moving by \sim 3 mm) to deliberately "spoil" the parallelism of the light at the filter, the sensitivity modulation is reduced to an acceptable level, orange.

Eleven input fibres of 1 mm diameter are stacked vertically on 1.4 mm centres. The 0.4 mm between fibres gives unambiguous track-to-track separation in the detector images and allows for some differences in image height between different gratings. Cemented achromats (Thorlabs AC508-100-A-ML) with a focal length of 100 mm and clear aperture >45 mm are used in a telecentric configuration with the dichroic mounted at the system pupil. With a total image height of the fibres of ± 7 mm, the clear aperture of the lenses is sufficient to ensure that light at the full NA of the spectrometer (f/4.6) passes without vignetting. The dichroic has a clear aperture of 46 mm and hence is oversize. The optics are required to be telecentric (such that the axial rays of edge fibres are parallel to the spectrometer optical axis) to avoid vignetting later within the system as rays from the edge of the object field pass through the spectrometer. Placing the dichroic at the telecentric pupil also serves to minimise the range of angles incident on it and hence maintain sharpness of its transmission band; however, during testing of the spectrometers, a modulation in system throughput of about 6% was measured varying with wavelength with a period of about 5 nm. This was attributed to etaloning in the dichroic support glass and due, in part, to the highly collimated light at the filter, Fig. 4. Moving the positions of the collimating (and focusing) lenses at the input optics by about 3 mm degraded the collimation enough that the sensitivity modulation was reduced to less than 1%.

IV. SPECTROMETERS

The requirements on the spectrometers for the new system were as follows: a high aperture to best match the fibres (NA 0.22), imaging/stigmatic to allow fibre stacking of fibres at the input slit and multiple tracks on the detector, sufficient spectral resolution (\sim 0.1 nm to resolve the Doppler shifted Stark features and Zeeman-split D_{α}), and compact, to fit the available space. Several commercial instruments with similar performances were compared, but the Princeton Instruments Isoplane device was a good match to our requirements

(we also had experience of interfacing this instrument to our control and data acquisition systems). This instrument also offered remote grating exchange with a choice of three gratings which, although not essential in our application, does give slightly more flexibility. The spectrometer achieves its stigmatic imaging through the use of an aspheric correction mirror placed after the grating. The correction is optimised for a grating angle of 17.68°. At higher grating angles, an asymmetry in the instrument function appears, as shown in Fig. 5.

Although one purpose of the upgrade was to provide the capability for simultaneous measurements of two wavelengths $(D_{\alpha}$ and impurity charge-exchange), it was also a requirement that this be achieved with no loss (and preferably a gain) in system throughput compared to the Czerny-Turner instruments that it replaced. The system throughput can be traded against spectral resolution by operating at different entrance slit widths; therefore, the relevant figure of merit (FOM) is the ratio throughput/slit-width. The throughput expresses the fraction of light from a fibre that reaches the detector plane and includes the degree of overfilling of the spectrometer aperture, the fraction of the fibre area that enters the slit, losses in the spectrometer (grating and mirrors or lenses), and losses in output matching lenses. The slit width is expressed in wavelength units using the dispersion (which is dependent on the grating ruling frequency and the instrument focal length). The predicted figure of merit for the new spectrometers is compared in Table I to the old, long focal length, spectrometers and to that of the HoloSpec fixed-wavelength instruments which view the opposite direction (opposite Doppler shift). The measured performance is discussed later.

The output plane of the spectrometers is 14 mm high and 27 mm wide which is well matched to a 1024 pixel CCD

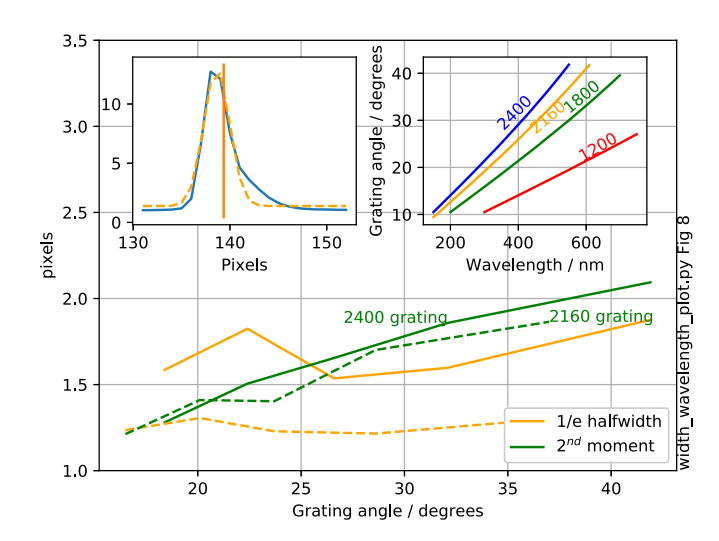


FIG. 5. Measured line shape broadening as a function of grating angle for two gratings. The left inset figure demonstrates the instrument line shape from a mercury line at 550 nm with the 2400 l/mm grating (grating angle of 42°). The linewidth is determined either by fitting a Gaussian to the profile (orange dashed line in the inset figure) or by computing the square root of its second moment $[\sqrt{\sum y_i(x_i-x_0)^2/\sum y_i}$, where x_i is the pixel number, y_i is the counts in that pixel, and x_0 is the position of the line centre from the first moment, orange vertical line] which is slightly more sensitive to asymmetries. The right inset plots the variation of the grating angle with spectrometer wavelength for various gratings. ¹⁰

TABLE I. Expected figure of merit (FOM) defined as the theoretical instrument throughput divided by the entrance slit width expressed in wavelength units. The dispersion is measured at the exit of the spectrometer and excludes the optical demagnification onto the sensor.

Instrument	NA	Grating	Dispersion (nm/mm)	Slitwidth (nm)	FOM (arbitrary)
Isoplane	0.11	2400	0.85	0.08	1.47
SPEX-KS5b	0.05	1800	0.28	0.22	0.82
HoloSpec-KS5d	0.28	holo	1.83	0.08	2.76

camera (with 16 μ m square) pixels. However, row transfer times for this sensor size are typically 1 μ s, which with our typical exposure times of 5–10 ms results in very high image-to-track smearing (the ratio of the image transfer time to track exposure time). Therefore the system is designed to use cameras with 512 pixel sensors, where the reduced electrode capacitance allows faster row transfer times of 0.3 μ s which with half the number of rows over which to shift the image results in only ~3% image-to-track smearing. The two impurity charge-exchange instruments reused our existing Andor iXon cameras, with the two new D_{α} spectrometers using new Princeton Instruments ProEM cameras. The cameras are coupled with 2:1 demagnification optics to the output of the spectrometer, as described in Sec. V.

The figure of merit measurements, Fig. 6, show that the new spectrometers approach the performance of the high throughput HoloSpec instrument. The performance of the old Czerny-Turner instruments is poorer than expected (based on Table I), probably due to a combination of factors including deterioration with the age of the reflecting components of the instruments.

The Isoplane entrance slit is set to 100 μ m which dominates the instrument function. However if an entrance

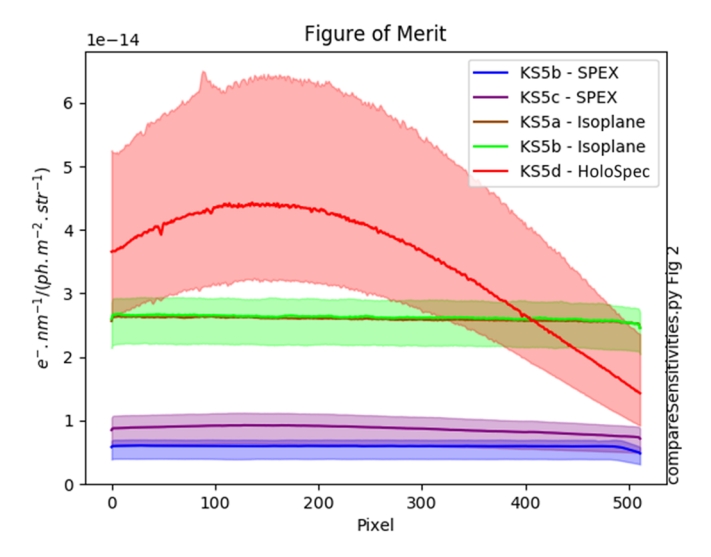


FIG. 6. Sensitivities of the Isoplane-based spectrometers, measured at 527 nm with the 2400 l/mm grating using an in-vessel light source (green and brown lines). The plotted curve is the median track with the shaded region spanning the 20-80 percentiles. Blue and purple curves are those of the old 1 m SPEX instruments and red is that of the HoloSpec transmission grating instrument (single slit configuration²).

slit narrower than about 70 μ m is used, then the intrinsic resolution of the spectrometer becomes the limiting factor. This design of the spectrometer is capable of better performance but only if the grating angle is close to its design optimum. With the high dispersion of 2400 l/mm grating and at 550 nm, the grating angle is at ~40° (close to the mechanical limit of the grating mechanism) where the stigmatic correction is incomplete and the line profiles are degraded, Fig. 5.

An additional spectrometer and a CCD camera have been installed with a single input fibre intended to achieve high throughput at high resolution. The instrument is fitted with a fibre optic image transformer at the entrance slit that converts the round 1 mm diameter fibre from JET to a line image 13 mm high and 65 μ m wide with a packing fraction of ~60%.

A. Grating choices

The fundamental constraint affecting the choice of grating is to obtain as large a dispersion as possible at the operating wavelength but with sufficient spectral range to be able to cover all the features of interest. The spectral range of the D_{α} system is required to cover the full Doppler shifted beam emission seen with simultaneous viewing from the red- and blue-shifted directions. For the impurity system, the spectral range has to allow for simultaneous recording of the C n = 8-7 and C n = 11-10 features at 529 and 525 nm and for the C n = 6-5 and C n = 8-6 features at 466 and 469 nm. In addition, sufficient spectral range must be available to allow for a good assessment of the spectral baseline to be obtained. (If the spectral baseline is poorly established, then determination of the spectral linewidth of the fitted lines is compromised.)

A large dispersion allows the use of larger entrance slits for the same wavelength resolution which increases the optical throughput of the system. However two factors argue against the use of higher ruling frequency gratings: grating reflectivity tends to be lower for high groove densities and when operating the spectrometers at grating angles higher than the designed 18° the instrument resolution deteriorates, as discussed earlier.

For charge-exchange measurements of light impurity spectral lines in high temperature (1–10 keV) JET plasmas, linewidths of 0.3–1.2 nm are typical and so an entrance slit width of $\sim 100~\mu m$ would be used. This is equivalent to 3 pixels at the detector; hence, a grating rotation angle of 30° is tolerable. Hence operation with a 2160 l/mm grating and perhaps 2400 l/mm grating is probably possible.

Since the spectrometers can be fitted with up to three remotely interchangeable gratings, we have selected the combination of 2400/2160/1200 l/mm gratings for the impurity charge-exchange instruments. We anticipate routinely using one of the two higher ruling frequency gratings (with the choice dependent on grating efficiency and achieved line shapes) but maintain the 1200 l/mm grating for high resolution work. The instruments for main ion spectroscopy are further constrained in that the D_{α} line at 656 nm lies beyond the 40° maximum grating angle for the 2400 l/mm grating, so these spectrometers have been equipped with 1800 and

2160 l/mm gratings. The single channel instrument is fitted with 1800, 2160, and 2400 l/mm gratings for maximum flexibility.

V. CAMERA COUPLING OPTICS

Coupling the output image of the spectrometers onto the 8 mm square CCD sensor in the 512 pixel cameras requires an image demagnification of 2:1. The requirement for this image reduction is for high image quality, with a flat focal plane, free of chromatic and geometric aberrations. The design and manufacture of such a system with bespoke optics would be expensive and time consuming. Instead a solution using commercial camera lenses was sought; however, the tilt of the spectrometer output plane introduces certain complications.

The output image plane of the Isoplane spectrometer is tilted by 14° from perpendicular to the instrument optic axis. Therefore, to achieve focus from one end of the spectrum to the other at the CCD sensor, the demagnification optics have to satisfy the Scheimpflug condition. This is achieved with the lenses aligned along the spectrometer optic axis but with the camera plane tilted at $7^{\circ} = \arctan(m \tan(14^{\circ}))$, where m = 0.5is the demagnification of the system. A further constraint is that the output lens configuration should be telecentric such that the demagnification is independent of the distance of an object point from the lens plane. If this condition is not satisfied, then the demagnification changes from one end of the spectrum to the other, leading to keystoning in the image, manifested as an up or down slope in spectra at the top and bottom of the CCD. These two constraints were satisfied using a pair of lenses with focal lengths of 100 mm and 50 mm—a Canon EF Series f/2 100 mm lens with a Zeiss Planar f/1.4 50 mm machine vision lens (M42 screw mount). These lenses are sufficiently compact that they could be fitted within a Thorlabs 60 mm cage system with only slight modifications to the two cage plates mounting the lenses. Since the internal optical configuration of the commercial lenses is proprietary information, the correct separation for the telecentric condition cannot be established with raytracing and had to be determined experimentally. At a separation between the front surfaces of the two lenses of 50 mm, the keystoning across the image was reduced to less than one pixel. This telecentric (or afocal) configuration corresponds to a Keplerian telescope. 11 In such a system, the lens principal planes are separated by the sum of their focal lengths. The (de-)magnification is given by the ratio of the focal lengths. The optical apertures of the two lenses have to be sufficient to avoid vignetting of the image. The sensor is 8×8 mm, i.e., 11.3 mm diagonal and the f-number of light onto the sensor 2.25 (half that of the spectrometer). Hence, to avoid vignetting at the corners of the sensor, the second lens must have an f-number no greater than 1.49. Similarly for the first lens, with an object diagonal at the spectrometer output of 22.6 mm and f-number of 4.5, the f-number of the lens should not exceed 2.23. The lenses selected approximately satisfy these criteria with some slight vignetting possible at the extreme corners of the field.

VI. CONCLUSION

An upgrade to the JET charge-exchange spectrometer has been implemented with the primary goal of giving simultaneous measurements of light impurity and fuel ion temperatures and velocities. The new impurity instruments also show a significant improvement in both throughput and instrument function compared to the previous Czerny-Turner instruments that they replace.

ACKNOWLEDGMENTS

This work has been carried out within the framework of the EUROfusion Consortium and has received funding from the Euratom research and training programme 2014-2018 under Grant Agreement No. 633053. The views and opinions expressed herein do not necessarily reflect those of the European Commission.

Work supported, in part, by the U.S. DOE under Contract No. DE-AC05-00OR22725 with UT-Battelle, LLC.

¹M. G. von Hellermann et al., Phys. Scr. **T120**, 19 (2005).

²S. Menmuir et al., Rev. Sci. Instrum. **85**, 11E412 (2014).

³E. Delabie et al., Plasma Phys. Controlled Fusion **52**, 125008 (2010).

⁴B. A. Grierson *et al.*, Phys. Plasmas **19**, 056107 (2012).

⁵E. Delabie *et al.*, in *Proceedings of 44th EPS Conference on Plasma Physics* (ECA, 2017), Vol. 41F, P4.159.

⁶C. R. Negus, C. Giroud, A. G. Meigs, K.-D. Zastrow, and D. L. Hillis, Rev. Sci. Instrum. 77, 10F102 (2006).

⁷C. Giroud, A. G. Meigs, C. R. Negus, K.-D. Zastrow, T. M. Biewer, and T. W. Versloot, Rev. Sci. Instrum. **79**, 10F525 (2008).

⁸R. E. Bell, Rev. Sci. Instrum. **75**, 4158 (2004).

⁹D. L. Hillis, D. T. Fehling, R. E. Bell, D. W. Johnson *et al.*, Rev. Sci. Instrum. **75**, 3449 (2004).

¹⁰See https://www.princetoninstruments.com/calculators/grating-dispersion. cfm for Princeton Instruments grating calculator.

¹¹W. B. Wetherell, "Afocal systems," in *Handbook of Optics*, 2nd ed. (McGraw-Hill, Optical Society of America, 1995), Vol. II, Chap. 02.